Analyses and Solutions for the Buckling of Thin and Flexible Electrostatic Inchworm Climbing Robots

Hongqiang Wang and Akio Yamamoto

***Abstract*—Planar and flexible climbing robots suffer from buckling while climbing on a vertical surface. This paper analyzes two different modes: one-end free buckling and two-ends fixed buckling. As an example for buckling analyses, the paper focuses on an electrostatic climbing robot that features thin body. As the body of the robot has only 2.5 mm of thickness, it is more prone to buckling than any other flexible robots, making it the best example for the buckling problem. Based on the analyses, the paper proposes a buckling-free control strategy for the electrostatic robots. The proposed strategy guarantees the force balance between adhesive force and weight force, as well as the elastic stability of the robot. To implement the strategy, the paper investigates the available region of the proper forces and optimal parameters on the prototype robot. A prototype of climbing robot was developed to verify the analyses and solutions, weighing merely 29 g (excluding battery and control circuits). It successfully climbed up a vertical wall without buckling, carrying the payload of 0.4 N.**

***Index Terms*—Climbing robot, elasticity stability, electrostatic adhesion, electrostatic film actuator, narrow gap.**

I. Introduction

THIN and flexible robots are gaining more and more attention, such as printable robots and origami-inspired robots [1]–[3]. Their compact bodies allow them to work in confined spaces such as human body cavities for surgery [4] or to be packaged into a small size for space deployment [5]. This paper focuses on thin and flexible climbing robots, which are highly desired in many applications such as inspection in the gaps of large machines [6]–[8]. The main challenges about this kind of robots are on two aspects: the actuator and adhesive devices. In previous research, conventional electromagnetic motors are usually employed for actuation and magnets for adhesion [6], [7]. Although they can provide quite a strong force, their great volumes and weights result in the problem of large sizes and energy waste. Therefore, other low-profile and lightweight actuators and adhesive devices should be considered.

Electrostatic film actuators [9]–[11] and electrostatic adhesion [12]–[14] are quite promising for this case. Since they both are made by plastic films with fine electrodes inside, the robot body can be compact. Compared to other new actuation methods such as shape memory alloys [15], dielectric actuators [16], and ionic polymer–metal composites [17], electrostatic actuators are easier for open-loop position control and stronger on output force [9], [10]. In contrast to other new adhesion methods such as directional adhesion [18], electrostatic adhesion is quicker in clutch/release and easier in fabrication [12], [13]. With these two techniques for actuation and adhesion, respectively, we can make the climbing robots, ultrathin, lightweight, and deformable. As shown in Fig. 1, containing only flexible electrode films and no rigid component, the prototype developed in this paper measures merely 2.5 mm in thickness, weighs 29 g, and can comply with complex profiles.

However, one of the critical problems for planar inchworm climbing robots lies on that the slim body is prone to buckle, resulting in the failure of climbing. As shown in Fig. 2(a), when the robot is borne by the hinder foot, the middle body will be compressed by two forces: supporting force from the supporting foot and the weight. Depending on different distribution and magnitudes of the gravity force, the planar body might buckle in two different modes, as shown in Fig. 2(b) and (c). An electrostatic inchworm climbing robots with an ultrathin body is a typical example suffering from this problem. Fig. 3 shows the whole failure process of buckling. Due to the compression, at a critical stroke, the slim films of the body will buckle, and then the falling front foot will peel off the adhering film from the substrate. Hence, the whole failure process can only be avoided by preventing the start of the buckling.

The purpose of this paper is to solve the buckling problem of the flexible electrostatic climbing robot on a vertical wall, a critical challenge ahead of field tests and practical applications. Considering planar robots generally suffer from the similar problem, this paper also aims to provide general analyses, models, and solutions. In this paper, simplified buckling models are built for different buckling forms. Depending on these models, a practical solution is proposed, including a new control strategy and selection method of the control parameters. This paper designs and fabricates a prototype of electrostatic climbing robots and verifies the concept and analyses with it.

Manuscript received December 11, 2016; revised March 23, 2017; accepted March 24, 2017. Date of publication April 18, 2017; date of current version August 7, 2017. This paper was recommended for publication by Associate Editor K.-J. Cho and Editor I.-M. Chen upon evaluation of the reviewers' comments. *(Corresponding author: Hongqiang Wang.)*

H. Wang is with the School of Engineering and Applied Sciences and Wyss Institute for Biologically Inspired Engineering, Harvard University, Cambridge, MA 02138 USA (e-mail: hongqiangwang@g.harvard.edu).

A. Yamamoto is with the Department of Precision Engineering, The University of Tokyo, Tokyo 113-8656, Japan (e-mail: akio@aml.t.u-tokyo.ac.jp).

This paper has supplementary downloadable material available at http://ieeexplore.ieee.org, provided by the author. The material consists of a video, viewable with Window Media Player 10. The size of the video is 20.6 MB. Contact Hongqiang Wang (hongqiangwang@g.harvard.edu) for further questions about this work.

Color versions of one or more of the figures in this paper are available online at http://ieeexplore.ieee.org.

Digital Object Identifier 10.1109/TRO.2017.2690302

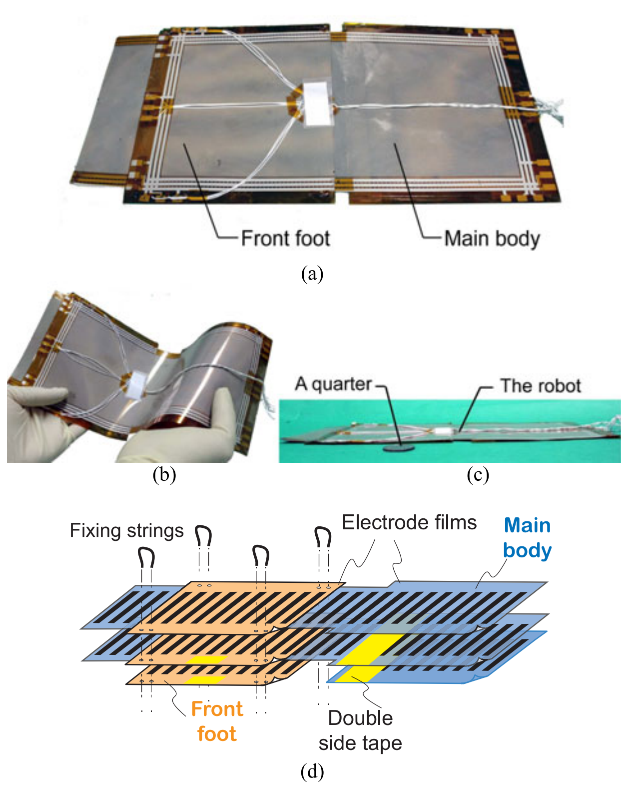

Fig. 1. Prototype of the inchworm climbing robot: (a) Upper view, (b) demonstration of its flexibility, (c) lateral view, and (d) structure of the robot.

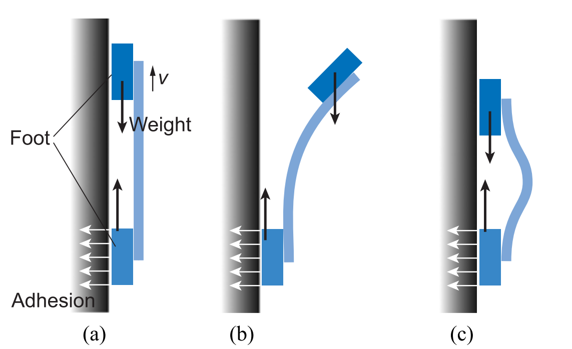

Fig. 2. Buckling of a planar inchworm climbing robot: (a) Forces on the robot. (b) and (c): Two possible buckling modes.

Since this kind of robots is composed of only flexible films, no rigid component, they are thin, flexible, and lightweight. They will be applicable for the inspection in narrow gaps or on curved surfaces, as alternatives to the conventional robots. These robots, with the sheetlike forms and weights of less than a hundred grams, can also benefit the safety to human beings and environment while they scale a building in a city.

The structure of this paper is as follows: the next section introduces the basic mechanisms in the electrostatic inchworm climbing robot, and then, in Section III, we analyze two main buckling modes of inchworm climbing robots, and discuss possible solutions and propose a new control strategy. Section IV analyzes the requirements on the forces and selects the proper parameters. Section V explains the fabrication of electrode films

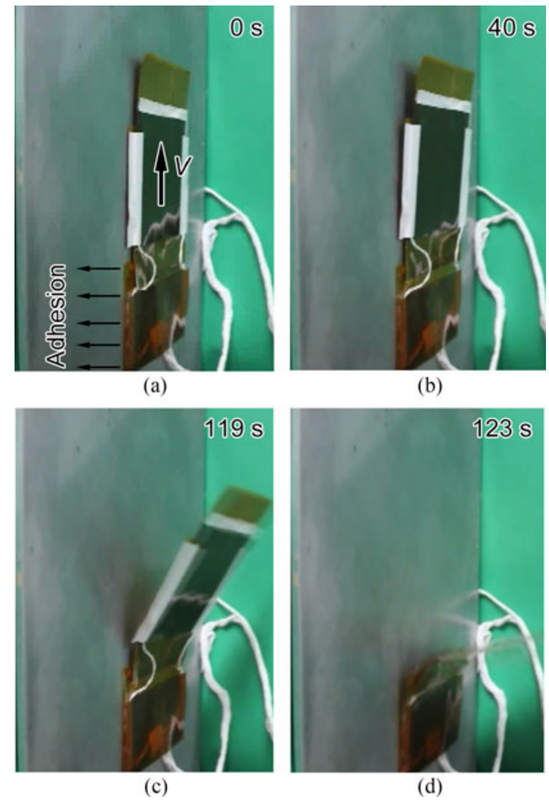

Fig. 3. Snapshots of the buckling process of a “fully electrostatic” inchworm-type climbing robot on a vertical aluminum plate. (a) Front foot is driven to move forward. (b) Buckling starts when the waist is too long. (c) Front foot section continues falling and bending the waist. (d) Dropping part of the front foot starts to peel the adhesive section. Noted the robot shown here is a primary prototype; the details about it can be found in our previous publication [19].

and describes the structure of the prototype of inchworm climbing robot and control circuit. Finally, in Section VI, experimental setup and results on the electrode films and climbing robot prototype are reported.

II. Basic Principles

A. Electrostatic Actuation

The electrostatic film actuators employed in this robot belong to the type of *dual excitation multiphase electrostatic drive* (DEMED) [9]. A typical DEMED actuator contains two identical films with embedded three-phase electrodes, as shown in Fig. 4(b). When three-phase voltage is supplied to the electrodes of both of the two films, the electrostatic force between the electrodes of the two films will drive the slider film to move.

The actuator works synchronously, and hence its speed is proportional to the voltage frequency [10]

$$v = 6\,pf \tag{1}$$

where p is the electrode alignment pitch between each two electrodes nearby, and f is the voltage frequency. One can control the velocity of the actuator by tuning the voltage frequency, change the velocity direction by altering the connection order

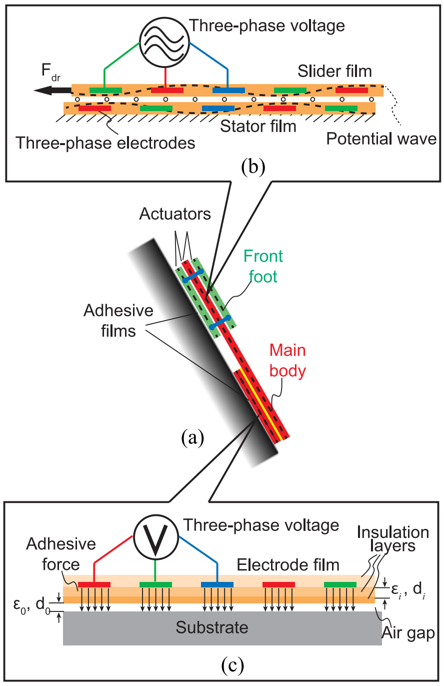

Fig. 4. (a) Conceptual design of the fully electrostatic inchworm climbing robot, (b) mechanism of electrostatic film actuation, and (c) principle of electroadhesion.

of the three phases, and clutch the actuator by supplying dc voltage instead.

The driving force of an electrostatic actuator is decided by [10]

$$F_{\rm dr} = K_{\rm dr} V^2 \tag{2}$$

where $K_{\rm dr}$ is the force coefficient of the actuator, and V is the zero-to-peak ac voltage. The driving force of the actuator can be increased by simply stacking more electrode films. For instance, an actuator stacking N pieces of films will generate $N-1$ times of force. By this way, this paper can achieve a stronger driving force than the adhesive force on the front foot of the robot, with the same voltage amplitude and same area.

B. Electrostatic Adhesion

Using electrostatic force, electrodes covered by insulation layers can adhere to a substrate [12], [13], as shown in Fig. 4(c). The electrodes can have many different patterns. The simplest one is a plane electrode connected to a dc high voltage, but the substrate should be grounded, which cannot be always guaranteed in practice. Two or more electrodes with different potentials can avoid grounding the metal substrate [12], [13], [20], [21]. This paper employs a layout with linear electrodes of three phases, the same as the ones used for the electrostatic actuators, to facilitate fabrication. Either dc or ac voltage can be supplied to the electrodes to activate the adhesion.

The adhesive energy per area can be calculated by

$$\bar{E}_{\rm ad} = a\varepsilon_0 \frac{w}{p} \frac{V^2}{\sum \frac{d_i}{\varepsilon_{\rm ri}} + d_0} \tag{3}$$

where $\varepsilon_{\rm ri}$ and d_i are the relative permittivity and thickness of the ith insulation layer, as shown in Fig. 4(c), ε_0 and d_0 are the relative permittivity and thickness of the air gap, respectively, V is the amplitude of the three-phase voltage, and a is the factor determined by the type of supplied voltage. If the voltage is three-phase dc ($+V$, 0, $-V$), a will be 1/3, and if it is ac, a will become 1/4. In this paper, the adhesive film attached to the main body is excited by dc voltage only; the front foot is activated by either ac or dc voltage depending on different locomotion phases. This will be explained in detail in Section V.

Based on the adhesive energy, the adhesive force per area can be calculated by

$$\bar{F}_{\rm ad} = a\varepsilon_0 \frac{w}{p} \left(\frac{V}{\sum \frac{d_i}{\varepsilon_{\rm ri}} + d_0} \right)^2. \tag{4}$$

On a vertical surface, friction force resulted from the adhesive force is relied on to support the robot. Its maximum value can be, if the friction coefficient is μ,

$$F_{f-\max} = \mu F_{\rm ad}. \tag{5}$$

C. Conceptual Design of the Fully Electrostatic Inchworm Robot

The fully electrostatic inchworm climbing robot integrating electrostatic actuation and electroadhesion is made of pieces of electrode films, no rigid mechanical structures. Fig. 4(a) shows a conceptual design.

The robot contains two independent components, referred to as the main body and the front foot, respectively. In the conceptual design shown in Fig. 4(a), the main body is inserted into the front foot. The front foot is composed of two short electrode films, and the main body is composed of a long film and a short film. The films of the front foot and main body together make up the actuator of the robot, which can drive the front foot or the main body to move forward. The films underneath the front foot and the main body are adhesive films, which can support the robot on a slope or wall.

In the designing, for compactness, the adhesive film of the front foot is also a part of the actuator. This means, when the adhesion and actuation are both activated on the front foot, the only voltage option is three-phase ac. On the other hand, if dc voltage is supplied to the all films of the front foot, the actuator will be blocked and only adhesion will work.

D. Locomotion of the Robot

The robot can move step by step just like an inchworm, by alternatively driving the front foot and the main body, as shown in Fig. 5. In each locomotion cycle, the robot has four locomotion phases: moving the front foot, stopping all the components, moving the main body, and stopping again.

Let v and L denote the velocity and stroke of the actuator in a moving phase, respectively, and t_0 is the time length for each stop phase. The average velocity of the inchworm robot can be

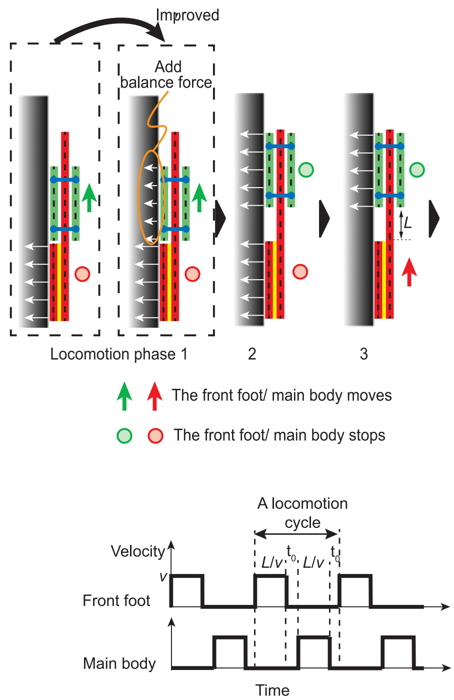

Fig. 5. (a) Locomotion phases of the previous control strategy in [10] and the new control strategy (introduced in Section III), and (b) timing diagram.

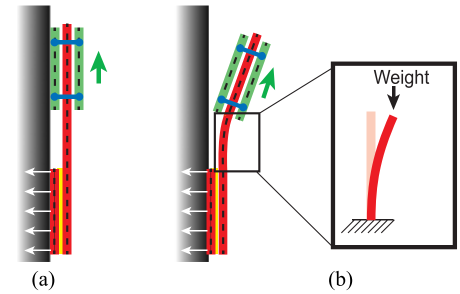

Fig. 6. Buckling with one end free, including (a) desired movement of the robot using the previous control strategy, (b) buckling of the upper section, and (c) analysis model.

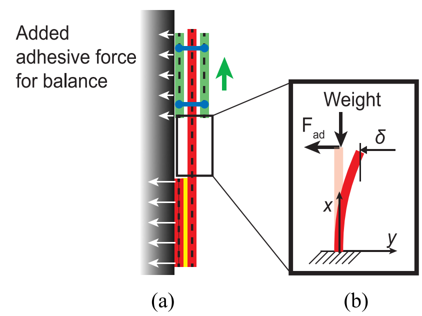

Fig. 7. (a) Solution to the buckling with one end free, and (b) analysis model.

calculated by

$$\bar{v} = \frac{L}{2\left(\frac{L}{v} + t_0\right)}. \tag{6}$$

III. Elasticity Stability of the Inchworm Robot and the New Control Strategy

When the front foot of the inchworm robot moves upward, the waist section made of electrode films is under compression, and bulking is apt to take place. Corresponding to the force conditions on the flexible climbing robot, buckling occurs in different modes. The mechanisms and solutions of two main modes are discussed in this section, and a new control strategy is proposed as a solution.

A. Buckling With One End Free

In the first locomotion phase, as shown in Fig. 6, the previous control strategy results in the buckling of the waist. The force model and solutions can be found in the following.

1) Analysis Model: Buckling with one end free can be simplified into the model that one film buckles with only one edge clamped, as shown in Fig. 6(c). This model only considers the deformation of the middle part of the main body, so-called "waist," but neglects the bending of the front foot section, due to two reasons. First, the front foot section is much more rigid than the waist, since the front foot section stacks more than twice films and have external wires and tapes attached on it. Second, the waist is subject to much stronger compressive force caused by the weight. Therefore, the buckling on the waist is dominant in buckling with one end free. This simplified model was verified in the experiments described in Section VI.

The critical buckling force can be derived, with the similar method based on energy conservation mentioned in [22] and [23], as

$$F_{\mathrm{crI}} = \frac{\pi^2 Db}{4L^2} \tag{7}$$

where D is the flexural rigidity per width of the film, L is the length of the waist, and b is the width of the film.

2) Possible Solutions: Based on the model, one can change the parameters in (7) to avoid buckling of the upper section. For example, we can limit the stroke of each step to reduce L or change the materials and stack more films to increase D. However, the former solution will decrease the velocity much according to (6), and the latter approach will deteriorate the desired characteristic of flexibility of the robot.

This paper proposes to add an adhesive force under the front foot while the front foot moves, as shown in Fig. 7. The critical voltage for this adhesive force is discussed as follows.

Due to the constraint conditions, the deflection curve can be given by [22]

$$y = \delta\left(1 - \cos\frac{\pi x}{2L}\right) \tag{8}$$

where δ is the deviation as shown in Fig. 7.

The total potential energy is the sum of the elasticity energy of the bended film, the work done by the compression force, and the change of the adhesive energy is given as

$$\Pi = U + T + \Delta E_{\mathrm{ad}} \tag{9}$$

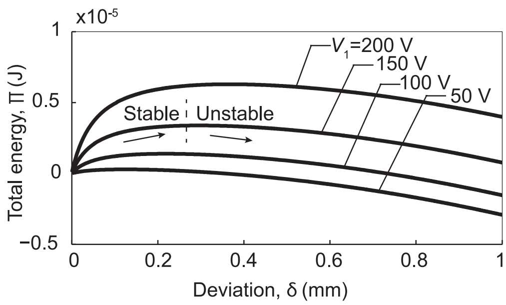

Fig. 8. Total energy for different deviations of an electrode film with a lateral balance force (the parameters are relative to the robot built in this paper: $D = 89\ \mu$N·m, $L = 30$ mm, $b = 125$ mm, $F_{\rm cr} = 0.195$N).

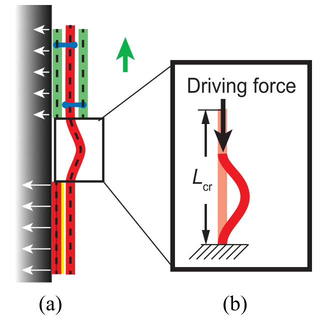

Fig. 9. (a) Buckling the "waist" of the inchworm climbing robot (buckling with two ends fixed), and (b) analysis model.

in which, $\Delta E_{\rm ad}$ is the decreased amount of the adhesive energy after buckling with a deviation of δ, which can be calculated by (3), assuming that the electrode pitch is small enough so that the adhesive energy is distributed continuously, and U and T can be calculated as [22]

$$U = \frac{Db}{2}\int_0^L \left(\frac{\partial^2 y}{\partial x^2}\right)^2 dx \tag{10}$$

$$T = -\frac{\delta^2\pi^2}{16L}F_{\rm cr}. \tag{11}$$

Due to energy conservation, if the total energy Π increases, the robot will be stable, and otherwise the robot will buckle. Based on (9)–(11), while the deviation grows, the total energy of the electrode film rises at first and then falls, as shown in Fig. 8. Theoretically, the robot will not buckle on a vertical surface regardless of the applied voltage because Π has positive inclination when the deviation is close to zero, buckling will not start in the beginning. However, in practice, an environmental disturbance might make the deviation exceed the stable range and trigger a buckling. As shown in Fig. 8, to ensure the stability, the maximum deviation of the stable status should be larger than the maximum deviation that an environmental disturbance might cause. Therefore, even affected by environmental disturbance, the robot can avoid buckling on a vertical surface by exciting enough adhesive force under the front foot.

B. Buckling With Two Ends Fixed

1) Analysis Model: To avoid the buckling with one end free, an adhesive force is added under the front foot during the moving period of the front foot. However, with this method, another mode of buckling is susceptible to happen instead. Different from buckling with only one end free, in this mode, both of the adhesive films stay at the substrate, but the waist buckle due to the compression of driving force, as shown in Fig. 9.

This mode can be modeled as a film with two opposite edges clamped. The buckling force in this mode can be calculated by the energy method [22]

$$F_{\rm crII} = \frac{4\pi^2 Db}{L^2}. \tag{12}$$

2) Possible Solutions: According to (12), to avoid the buckling with two ends fixed, we can enhance the rigidity of the robot or limit the stroke of the movement and compressive force. To keep the desired feature of flexibility of the inchworm robot, in this paper, the compressive force is constricted with the concern of an intentionally restrained stroke.

C. New Control Strategy

According to the solutions mentioned above, the new control strategy should be different from the common ones used for inchworm robots. To avoid buckling with one end free, the adhesion of the moving front foot should be activated to keep the balance of the upper section in locomotion phase 1, as shown in Fig. 5(a). On the other side, to avoid buckling with two ends fixed, the driving force and the stroke should be limited. The quantitative analyses are conducted in the next section.

IV. Force Analysis and the Parameter Selection of the Climbing Robot

Using the new control strategy, the performance of the robot will vary with different parameters. These parameters contain the pattern dimensions such as thickness of each layer and the voltages on different electrodes films in different locomotion phases. In some conditions, the robot might fail due to weak adhesion/actuation force or buckling problem. With these concerns, this section finds the safe region of parameters and optimizes the parameters.

A. Force Analysis of the Inchworm Climbing Robot

Considering the balance of the inchworm climbing robot as shown in Fig. 10, forces are analyzed in each of the four locomotion phases as follows.

In the first locomotion phase, the adhesive pad of the main body should exert adhesive force strong enough to support the whole body, and the actuator should be able to push the front foot upward

$$F_{f2-\max} \geq F_{f2} = F_{f1} + F_{\rm g} + P \tag{13}$$

$$F_{\rm dr-max} \geq F_{\rm dr} = F_{f1} + F_{g1}. \tag{14}$$

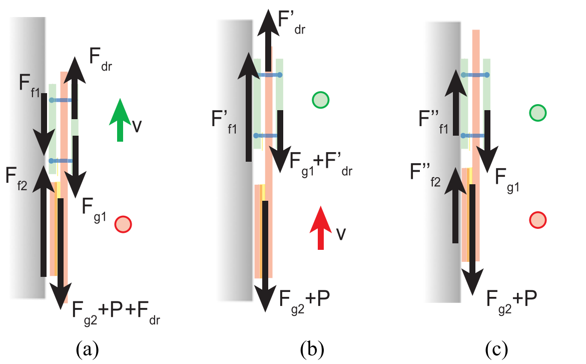

Fig. 10. Force analyses of the inchworm robot in the four locomotion phases: (a) Phase that the front foot moves; (b) phase that the main body moves, and (c) stopping phases.

Similarly, in the third locomotion phase, we have

$$F'_{f1-\max} \geq F'_{f1} = F_g + P \tag{15}$$

$$F'_{\mathrm{dr}-\max} \geq F'_{\mathrm{dr}} = F_{g2} + P. \tag{16}$$

If the force balances are fulfilled in the two moving phases 1 and 3, the forces will be balanced when the robot stops in phases 2 and 4, too. This is because in the stopping phases, two feet are utilized for the supporting, whereas in the moving phases, adhesion of only one foot is employed, as shown in Fig. 10(c).

On the other aspect, to avoid the two modes of buckling, respectively, the elasticity stability should be kept by, according to (7) and (12),

$$V_1 \geq V_{\mathrm{crI}} \tag{17}$$

$$F_{\mathrm{crII}} \geq F_{f1} + F_{g1}. \tag{18}$$

Only if the forces on the robot fulfill all of the above six equations, the robot can climb up a vertical surface; otherwise the robot will fail due to inadequate adhesion/driving force or excessive compression.

B. Parameter Selection

To achieve the forces limited by both force balance and elasticity stability, proper parameters should be selected, including the dimensional parameters of the electrodes films and the voltages.

Either the adhesive forces or driving forces can be generalized into the following form, according to (2) and (4),

$$F = KV^2. \tag{19}$$

To decide the dimensional parameters for the required friction forces and driving force, one can just decide the proper range of $K_{f\,1}$, $K_{f\,2}$, and K_{dr} instead. The symbols in this section are listed in Table I.

Equations (13)–(16) and (18) can be transformed into

$$K_{f2}V_2^2 \geq K_{f1}V_1^2 + F_g + P \tag{20}$$

$$K_{\mathrm{dr}}V_1^2 \geq K_{f1}V_1^2 + F_{g1} \tag{21}$$

TABLE I
PARAMETER DEFINITION IN THE FORCE ANALYSIS

Parameters	Definition
$F_{f\,1}/\ F'_{f\,1}$	The friction force between the front foot and the substrate in the first/third locomotion phase.
$F_{f\,2}/\ F'_{f\,2}$	The friction force caused by adhesion between the adhesive film attached to the main body and the substrate in the first/third locomotion phase.
$F_{\mathrm{dr}}/\ F'_{\mathrm{dr}}$	Driving force of the actuator in the first/third locomotion phase.
F_g	The weight of the whole robot.
$F_{g\,1}$	The weight of the actuator section.
$F_{g\,2}$	The weight of the main body.
P	The extra payload on the robot.
$V_{\mathrm{cr\,I}}/\ V_{\mathrm{cr\,II}}$	Critical voltage for buckling with one end free/ buckling with two ends fixed.
$F_{\mathrm{cr\,I}}/\ F_{\mathrm{cr\,II}}$	Critical force for buckling with one end free/buckling with two ends fixed.
V_1	Zero-peak voltage amplitude of the three phase voltage on the actuator films in locomotion phase 1.
V'_1	Amplitude of the three phase dc voltage channels (+V, 0, −V) in the third locomotion phase.
$V_2\ /\ V'_2$	The voltage on the adhesive film of the main body for adhesion in the first/third locomotion phase.
$K_{f\,1}/\ K_{f\,2}/\ K_{\mathrm{dr}}$	The representative coefficient of the force $F_{f\,1}/\ F_{f\,2}/\ F_{\mathrm{dr}}$.

$$K_{f1}V'^2_1 \geq F_g + P \tag{22}$$

$$K_{\mathrm{dr}}V'^2_1 \geq F_{g2} + P \tag{23}$$

$$F_{\mathrm{crII}} \geq K_{f1}V_1^2 + F_{g1}. \tag{24}$$

Therefore, the parameters should be limited by (17) and (20)–(24), and we have 13 parameters in total.

For the simplicity of analysis, F_{g1}, F_{g2}, and F_g are assumed to be constants. We can decide the eight parameters: K_{f1}, K_{f2}, K_{dr}, V_1, V_2, V'_1, V_{cr}, and F_{crII}, as follows.

First, since five independent variables (V_2, V'_1, K_{dr}, K_{f2}, $F_{\mathrm{cr\,II}}$) lie in only the left side of the inequalities, they should be as great as possible. For example, the voltages can be the maximum value without electric breakdown,

$$V_2 = V'_1 = V_{\max}. \tag{25}$$

In the following analysis, F_{g1}, F_{g2}, and F_g are assumed to be 0.12, 0.27, and 0.29 N, respectively. $V_{\max}$ is 600 V, K_{dr} is 3.2 μN/V^2, K_{f2} is 6.0 μN/V^2, and $F_{\mathrm{cr\,II}}$ is 0.76 N when the stroke L is constrained to 24 mm, corresponding to the electrode films fabricated in this paper. In the estimation for electroadhesion, the thickness of the air gap is assumed 15 μm based on preliminary experiments of adhesive force.

Now only three parameters are remained to be decided, K_{f1}, V_1, and $V_{\mathrm{cr\,I}}$. For the former two parameters, one can refer to the coordinate plane of (V_1, F_1), as shown in Fig. 11. The reasonable parameters should fall in the intersection of the two regions for elasticity stability [see (17) and (24)] and force balance [see (20) and (21)]. Since $V_{\mathrm{cr\,I}}$ is decided by $K_{f\,1}$ according to the analysis in Section III, we at first select $K_{f\,1}$ and V_1 only considering force balance, and then check whether the parameters satisfy elasticity stability relevant to $V_{\mathrm{cr\,I}}$ by (17). Note, when force balance is only considered, for different desired external payload, the available region changes as shown

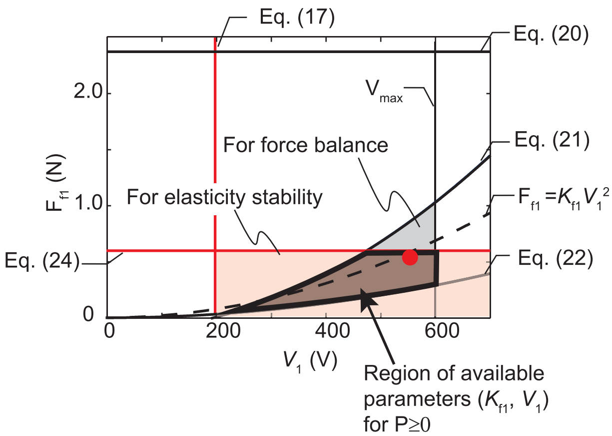

Fig. 11. Available range of (K_{f1}, V_1) for the robot climbing on a vertical surface without any extra payload.

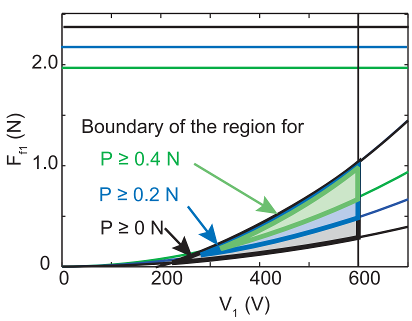

Fig. 12. Available regions of (K_{f1} and V_1) for the robot climbing on a vertical surface with different amounts of payload, only considering the force balance.

in Fig. 12. This paper chooses 2.2 $\mu N/V^2$ for K_{f1} and 550 V for V_1, shown as the red point in the intersection region of Fig. 11.

With the decided parameters, the payload capacity can be derived from the inequalities (20), (22), and (23)

$$P' = \min. \begin{pmatrix} K_{f2}V_{\max}^2 - K_{f1}V_1^2 - F_g \\ K_{f1}V_{\max}^2 - F_g \\ K_{\mathrm{dr}}V_{\max}^2 - F_{g2} \end{pmatrix}. \quad (26)$$

This equation illustrates that the payload will increase proportionally when the area of the robot increases.

V. Design and Fabrication of the Prototype

In the inchworm climbing robot, all the electrode films used are the same in the structure to simplify the manufacturing, as shown in Fig. 13. They are fabricated by screen printing and then cut into different sizes to construct the prototype of inchworm climbing robot. Each film contains a polyimide base layer (V100, Kapton), upper and lower resin cover layers (FR-1T-NSD9, Asahi), and linear electrodes printed by silver paste (MP-603S-5702-F, Mino), as shown in Fig. 14.

Using these electrode films, we fabricated the inchworm climbing robot as shown in Fig. 1. Its specifications are listed in Table II. This prototype contains two parts: the front foot and main body. The front foot stacks three electrode films, which

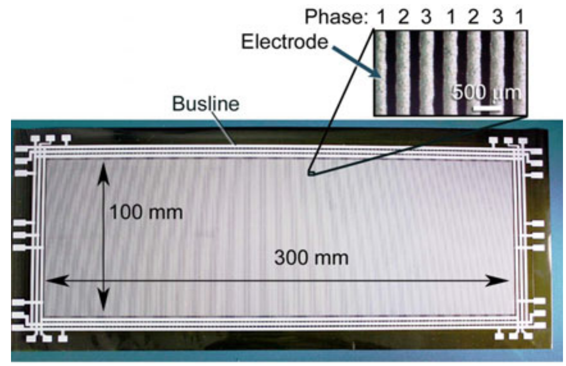

Fig. 13. Electrode film used in this paper.

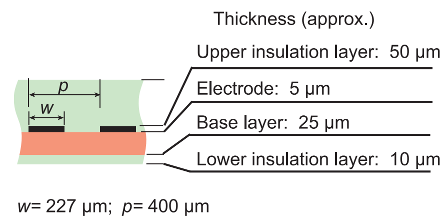

Fig. 14. Structure of the electrode film.

TABLE II
SPECIFICATIONS OF THE PROTOTYPE OF "FULLY ELECTROSTATIC" INCHWORM CLIMBING ROBOT

Spec.	Values
Area	298 mm × 135 mm
Height	2.5 mm (with wires) 1 mm (without wires)
Weight	29 g (excluding off-board battery and control circuits)
Effective adhesive area of each foot	100 × 100 mm^2
Maximum payload	0.4 N
Average speed	3 mm/s
Maximum voltage	600 V
Thickness of each electrode film	90 μm

were fixed by double-side tapes and strings. The strings also work as a holder to constraint the moving direction of the actuator. The main body is made of two long electrode films with an electrode area of 274 × 100 mm^2 for actuation, and one smaller electrode film of 100×100 mm^2 for adhesion. The front part of the main body is inserted into the front foot to compose four electrostatic actuators, as shown in Fig. 1. Every electrode film used in the prototype is arranged with the upper insulation layer being on the top side. Besides, to make K_{f1} to be the value selected in the last section, three-fourth area under the front foot was covered with acetate tapes (thickness: 60 μm, relative permittivity: 2). The friction coefficient of the tapes on the aluminum board is 0.26, and that of the electrode film on the same board is 0.36. For lubrication, glass beads were scattered between the electrode films of the actuator.

In the circuit, six channels of voltages are generated by a controller board (DS1104, dSPACE) and then amplified 1000 times by amplifiers (HVA4321, NF) to excite the climbing robot. Channels 4, 5, and 6 are supplied to the adhesive film of the main

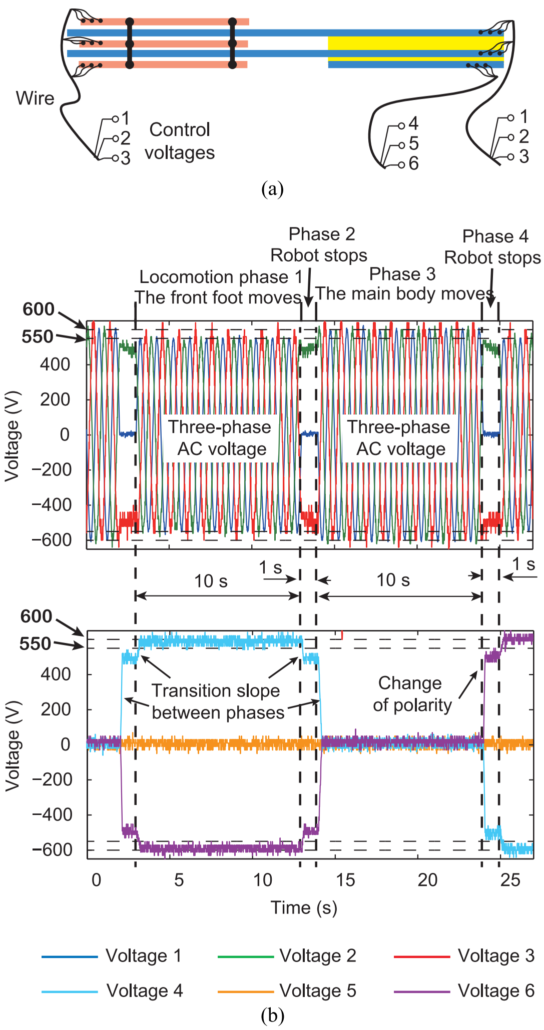

Fig. 15. Six channels of voltages supplied to the "fully electrostatic" climbing robot: (a) Wire connection on the robot; (b) change of the voltages on the six channels in the locomotion changes.

body for adhesion, while the other three channels are connected to the three-phase electrodes of the other films for actuation, as shown in Fig. 15(a). For the four locomotion phases, the voltages change as shown in Fig. 15(b). In the first locomotion phase, three-phase dc voltages (600 V, −600 V, 0 V), by channels 4, 5, and 6, activate the adhesive film of the main body, when three-phase sinusoidal ac voltages (600 V_{0-p}) power up the actuator and the adhesive film of the front foot by the other three channels. In the second locomotion phase, voltages for all the films are three-phase dc (500 V, −500 V, 0 V), while both of the two adhesive films clutch on the wall. Then, all the films of the front foot are supplied with three-phase sinusoidal ac voltages (600 V_{0-p}) to start up the actuator, meanwhile the voltages in channels 4, 5, and 6 for the adhesive film of the main body is grounded. Again, the robot stops at phase four by supplying all the phases with dc three-phase voltages (500 V, −500 V, 0 V).

To avoid corona discharge, the voltage should be lower than a critical value, ±600 V for the actuator based on tests due to the narrow space between electrodes. For adhesion, the voltage amplitude should also not overreach this value, since the adhesive film of the front foot is shared by the actuator simultaneously considering low profile of robot and ease of fabrication. On another aspect, sudden change should also be averted against discharge. Voltages between different locomotion phases are connected with transition slopes, as shown in Fig. 15. Besides, under dc voltage, charges will accumulate on the film surface and consequently deteriorate the adhesive force after a period [12], [13], [20]. To avoid this problem, this paper changed the polarity of the dc voltages (channels 4, 5, and 6) on the adhesive film of the main body after every locomotion cycle, as shown in Fig. 15(b). The adhesive film of the front foot uses three-phase sinusoidal ac voltages, but the adhesive film of the main body employs dc voltages. This is because the adhesive film of the front foot is part of the actuator simultaneously, whereas the adhesive film of the main body is applied only to adhere to the substrate. Three-phase voltages can activate both the electrostatic actuation and adhesion, and, on the other aspect, dc voltage can merely excite electroadhesion.

VI. Experiments

The buckling models were verified by experiments on electrode films and the inchworm robot. With the solutions to the buckling problem, the prototype was driven to climb up on a vertical surface successfully, and its displacement and payload were tested.

A. *Experimental Verification of Buckling With One End Free*

Buckling with one end free is simplified into a compressed cantilevered film and characterized by (7). Two aspects about this simplification need to be verified by experiments. The electrode films contain multiple layers of materials and interdigital electrodes, while the model assumes that the films' material is unformal, so the impact of the material should be clarified by tests. The other concern is that the whole robot is simplified into a simply clamped film, which needs to be justified. For the first concern, this paper tested the buckling force on electrode films clamped on one edge and compared the experimental results with the estimation. For the second concern, this paper located the inchworm robot on a vertical wall with/without voltage to verify the conducted equations in the simplified model.

1) Tests on the Electrode Films: In the experiments, the lower edges of the electrode films were fixed by a clamper, and the upper edges were pressed by a force sensor (LTS-1kGA, Kyowa for the force above 0.3 N, and LTS-50GA for the other values of force) with a parallelogram structure under the sensor, as shown in Fig. 16(a). This parallelogram structure, made of two parallel acrylic plates hinged by four links, is designed to reduce the influence of friction force between the acrylic plate and the upper edges of the films. With this structure, the friction force will waste negligible energy, and involve little in the energy transformation during the buckling process. The tested results are coincident with the analysis according to (7), as shown in Fig. 16(b), verifying the model for buckling with one end free.

Then, to test the possible influence of the internal voltage on the buckling force, we supplied 500 V_{0-p} three-phase ac voltage to the films, when there were two electrode films. No obvious

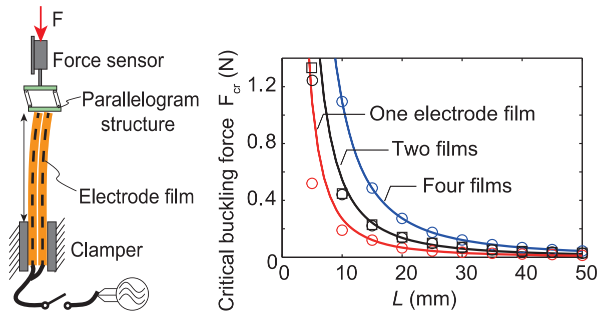

(a) (b)

Fig. 16. (a) Experimental setup for testing the critical buckling force of the electrode films with one side of edges clamped and (b) experimental results (lines indicate calculation results, circle markers represent experimental results on the films with no voltage, and square markers denote the electrode films excited by $500\,V_{0-p}$ three-phase ac voltage).

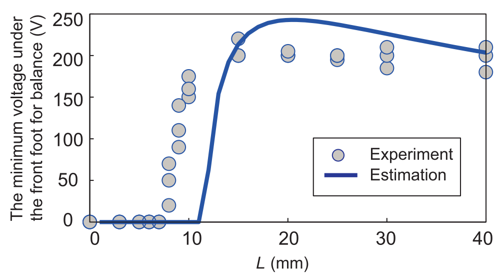

Fig. 17. Experimental results of the critical value of V_1 for the balance of the robot on a vertical surface with different lengths of stroke.

difference occurred on the critical buckling forces with voltage on and off. This suggests that it is safe to neglect the impact of voltage in the analysis of buckling force. In the estimation, the flexural rigidity D is 89 μN·m based on a simple cantilever test on the electrode film.

2) Tests on the Inchworm Robot: The inchworm robot was activated to attach to a vertical wall. The critical voltage on the front foot was acquired as a function of the waist length, to justify the model and solution characterized by (7) and (9), respectively.

The adhesive film of the main body, activated by three-phase dc voltage of 600 V, adhered to a vertical aluminum board. The front foot, which was fixed to the main body by tapes at an assigned position, was supplied with three-phase ac voltage. The amplitude of this voltage was changed, and when it was lower than a value (the critical voltage), the robot would buckle. For different length of waist, the critical voltage is plotted in Fig. 17.

Just as estimated by (8) and (9), if the length of the waist is too long, the robot cannot stand vertically anymore once there is not enough voltage on the front foot. With no voltage, the critical waist length in estimation (11 mm) is close to that of tests (7 mm), verifying the simplified model of buckling with one end free indicated by (8). When the front foot is supplied voltage, the trend of the critical voltage calculated by (9) also matches the experimental data. Once the length of the waist exceeds the threshold value, the critical voltage first increases

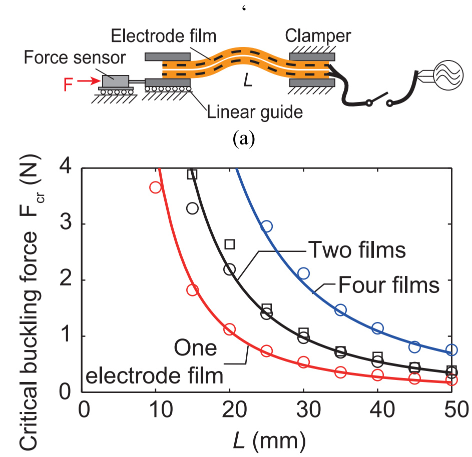

(a) (b)

Fig. 18. (a) Experimental setup for testing the critical buckling force of the electrode films with two edges clamped and (b) experimental results (square marker: the electrode films are supplied with $500\,V_{0-p}$ three-phase voltage).

steeply and then drops slowly. In this estimation, the deviation δ of the upper end of the waist is assumed as 0.4 mm. There is a little discrepancy between the experiment and simulation, due to two aspects. First, the elasticity of the front foot section is not considered in the model. Second, the wires and tapes attached on the front foot of the robot bring in extra weight and bending moment. For better estimation in the future, both these two aspects should be contained in the model, but the calculation will be much more complex. For the application in this paper, the current simplified model is accurate enough.

B. Experimental Verification of Buckling With Two Ends Fixed

1) Tests on the Electrode Films: To test the buckling with two ends fixed on the electrode films, two clampers were employed to fasten two opposite edges of the electrode films, as shown in Fig. 18(a). One clamper was fastened to a stage. The other one was located on a linear guide and pushed by a force sensor (LTS-2kGA, Kyowa) to compress the films between the clampers. The measured critical buckling force agrees to the analysis by the model, shown in Fig. 18.

2) Tests on the Inchworm Robot: To test the buckling with two ends fixed on the robot, the adhesive film of the main body was located on a fixed aluminum board, and the front foot was on another aluminum board with a linear guide underneath the board, as shown in Fig. 19(a). The front foot of the robot was activated by a three-phase ac voltage ($600\,V_{0-p}$), whereas the adhesive film of the main body was excited by a three-phase dc voltage (600 V), and hence these two components adhered to the aluminum boards with the electroadhesive forces. Then, the aluminum board was pushed on the guide by a force sensor (LTS-200GA, Kyowa) to compress the robot until the robot failed. In this test, the robot failed in two forms depending on the length of the waist, while the waist is shorter than 33 mm, the front foot slipped, but when the waist is longer than that value, the robot buckled, just as estimated, as shown in Fig. 19(b).

The estimations of the adhesive forces and the critical buckling force are according to (4) and (12), respectively. When we

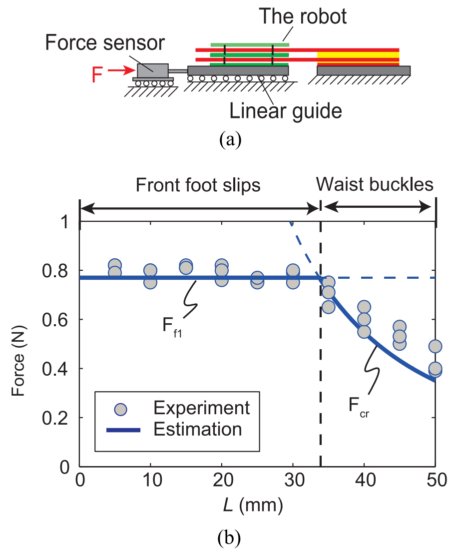

Fig. 19. (a) Experimental setup for the critical compressive force on the robot as each of the two feet is attracted on an aluminum board and (b) experimental results.

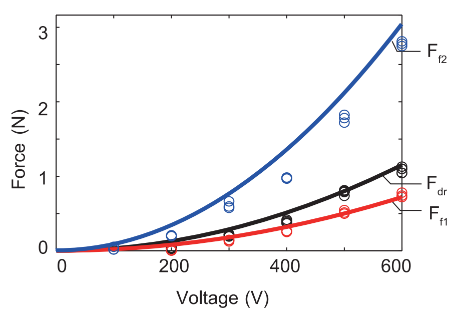

Fig. 20. Friction forces on the two feet and the driving force of the prototype for different voltages (circles: experimental data; lines: estimation from models).

calculate the friction force under the front foot, the effect of the front section's weight of the robot was also summed in.

The experimental results prove that when the length of the waist is short enough, the buckling with two ends fixed can be avoided, even though the robot body is under a compression, which essentially enables the robot to climb on a vertical surface.

C. Forces of the Robot

The friction forces under the adhesive films and the driving force of the actuator were tested, and the results are plotted in Fig. 20. When the friction force under the adhesive film of the main body was measured, the similar setup introduced in Fig. 19(a) was utilized. The front foot was fixed by tapes on the sliding board and the adhesive film of the main body (excited by voltage for electrostatic adhesion) located on the fixed board. Then, a force sensor (LTS-1kGA, Kyowa) pulled the front foot by a spring until the adhesive film of the main body slipped on the fixed board to acquire the friction force. In a similar way, the friction force under the front foot was tested. On another aspect, when the driving force was verified, the front foot on the sliding board was driven by the actuator of the robot to pull the fixed force sensor. In the experiments of this part, for F_{f1} and F_{dr}, the voltage is three-phase ac, whereas for F_{f2}, it is three-phase dc, just the same with the voltages used in the operation of the robot.

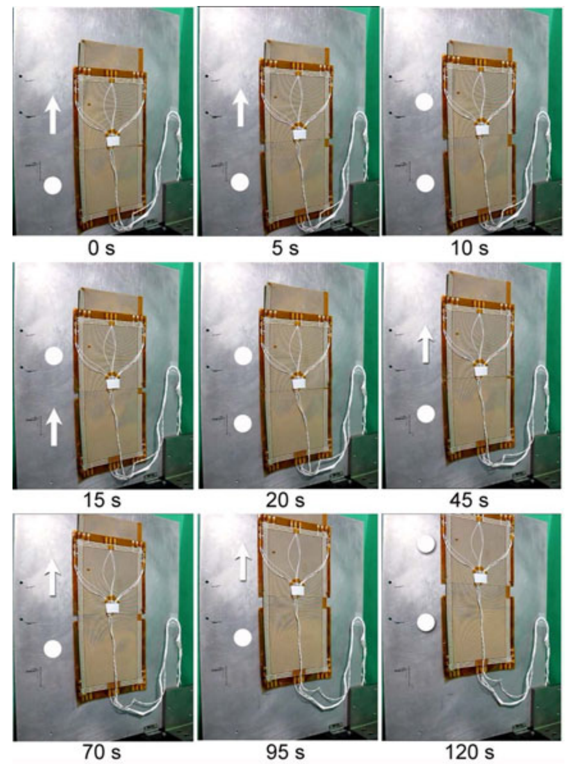

Fig. 21. Snapshots of the movement of the robot as it climbs up on a vertical aluminum board (circle marks mean that the corresponding component stops, and arrows mean that it moves).

Results of the forces in Fig. 20 verify the feasibility of the calculation. In the estimation of the driving force, the coefficient K_{dr} is $3.2\,\mu\mathrm{N/V}^2$, from preliminary test on a simple actuator composed of two electrode films. The figure also shows that, on the front foot, the driving force of the actuator is stronger than the adhesive force underneath the front foot, to ensure the moving up of the front foot with the adhesive force underneath.

D. Performance of the Robot on a Vertical Surface

With the new control strategy and proper parameters, the robot successfully climbed up a vertical surface of an aluminum board, without buckling anymore, as shown in Fig. 21.

Several problems were also observed. The adhesive force of the robot decreased after a period of movement, resulting from the glass beads. These glass beads were originally used for the lubrication of the actuators, but they were apt to drop out from the actuator and caused slip of the adhesive films. Hence, we had to clean the contact surfaces of the substrate and the robot after several trials. Another problem is that the actuator's driving force sometimes happens to be very weak. This is because, in the prototype, the moving direction of the actuator was constrained by the strings through every film of the front foot. These strings could not precisely limit the locomotion direction, but leave some free space. The main body of the robot sometimes tilted left/right with a small angle, resulting

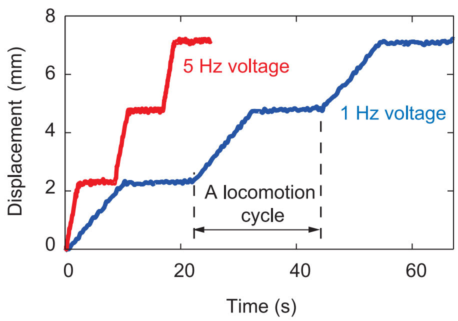

Fig. 22. Displacement of the front foot of the prototype.

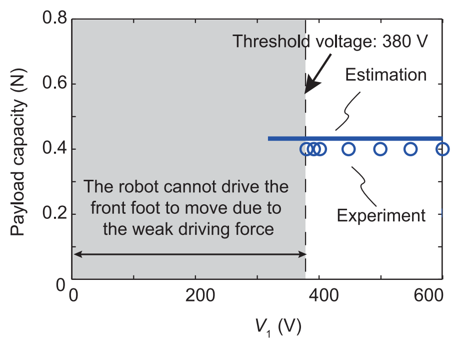

Fig. 23. Payload of the prototype for different V_1 (the robot can move only if V_1 is higher than the threshold value).

in the linear electrodes between different films unparalleled, and consequently deteriorated the output force strength. Similar phenomenon and its analysis can be found in [10].

E. Displacement of the Robot

The movement of the prototype robot was tested as it climbed up a vertical aluminum board. A laser sensor (ANR1215, Panasonic) was installed on the aluminum, and a reflecting marker made of a paper was attached on the front foot of the robot.

The displacement of the front foot is shown in Fig. 22. When the frequency of the voltage on the actuators is 1 Hz, the average velocity is 1.1 mm/s, the same to the estimated value by (6). In this test, the period for each moving phase is 10 s, and each stopping phase takes 1 s, as shown in Fig. 15(b). On the other side, if the voltage frequency increases to 5 Hz, each moving phase takes 2 s, and each stopping phase costs 2 s, the practical average velocity will be $3\,\mathrm{mm/s}$. The speed of the robot can be promoted more by increasing the voltage frequency of the synchronous actuator, but this will increase the risk that actuator fails to catch up the synchronous speed.

F. Payload of the Robot

This paper tested the prototype's payload by hanging weights on the prototype's main body and driving the robot to move on a vertical aluminum board. Since, as analyzed in Section III, the voltage V_1 is critical for the payload capacity, it was changed in the tests and the corresponding payload capacities were acquired, as shown in Fig. 23. It was observed that, if V_1 was small, the climbing robot's actuator could not drive the front foot to move in the first locomotion phase because the driving force was too weak to lift up the front foot's own weight. On the other hand, if V_1 exceeded 380 V, the robot can travel with the payload lower than 0.4 N, and once the payload was heavier than this value, the robot would slip in the third locomotion phase since the friction force under the front foot was not strong enough to support the total weight. The tested payload capacities are a little smaller than the calculation due to the weight of the wires and the deformation of the electrode films.

G. Discussion

The payload of the prototype in this paper is 0.4 N, although not so strong compared to the climbing robots with electromagnetic adhesion and motors, it is enough to carry miniature cameras or lightweight devices that are compact enough for working in a narrow gap. For example, one of the commercial available camera weighs only 0.2 g [24], and a circuit with wireless communication and controller using integrated electronics can be lighter than 3.2 g [25]. Even though the payload exceeds the capacity of this prototype, especially when the control circuits and battery are carried on in the future, the prototype can be re-built by simply scaling up the area without impact on the robot's thickness, since both its driving force and adhesive force are proportional to the area. In particular, we can increase the area of robot by five times to achieve 2 N payload, but this size needs larger screen printing machine and exceeds the capacity of our current equipment. Besides, compared to the electromagnetic adhesive devices, the weight of the robot is quite low, and hence, it costs less energy as lifted up and requires much smaller battery, which will benefit the working in a confined space.

In this paper, the substrate is a flat aluminum board. Of course, the robot is possible to adhere on various materials but the adhesion force will differ, according to previous literatures [12], [13]. On other metals, the robot can climb up with the corresponding parameters deducted from the same equations in Section IV; on nonconductive materials such as glass and wood, the adhesive films should be supplied dc voltage only and separated from the actuator, but the same control strategy and parameter selection method can still be utilized. The robot is also expected to move on a complex surface, not only on a flat surface, since the actuator and adhesive film can both work on a curved surface [9], [21], but the driving force might drop when the curvature arises [26]. This will be studied in the future.

VII. Conclusion and Future Works

To circumvent the buckling problem of the flexible fully electrostatic inchworm climbing robot and to make the robot be able to climb up on a vertical surface, this work built analysis models for two main buckling modes. Based on the models, two solutions were proposed, including 1) introducing an adhesive force under the front foot when it moves upward, to avoid the buckling of the upper section of the robot body, and 2) limiting the compressive force on the waist and locomotion stroke to avoid the buckling of the waist of robot with two ends fixed. Considering both force balance and elasticity stability, forces on the robot were analyzed and the parameter selection method for proper forces was investigated.

A prototype of fully electrostatic inchworm-type climbing robot was constructed using only flexible electrode films, without any rigid component. This prototype is light (29 g), low-profile (2.5 mm in height), and flexible. With the new control strategy and careful force control, the prototype can move on a vertical aluminum board successfully with a speed of 3 mm/s and carry a payload of 0.4 N at maximum.

For practical application, a lot of efforts are still required. In the future, larger films will be realized to streng then the payload by using larger screen printing machine or inkjet printer. A compact power source, a control unit, and several sensors for specific applications will be designed and installed, using the integrated electronics technique. Alternative lubrication methods, such as low-friction surface coating, will replace glass beads. Moreover, the study on the mechanisms of the flexible fully electrostatic inchworm climbing robot moving on a curved surface will also be conducted. More functions such as multiple moving directions will be updated to the robots in the future.

Acknowledgment

This work was carried out in the University of Tokyo.

References

[1] C. D. Onal, R. Wood, and D. Rus, "Towards printable robotics: Origami-inspired planar fabrication of three-dimensional mechanisms," in *Proc. IEEE Int. Conf. Robot. Autom.*, 2011, pp. 4608–4613.

[2] S. Miyashita, S. Guitron, K. Yoshida, S. Li, D. Damian, and D. Rus, "Ingestible, controllable, and degradable origami robot for patching stomach wounds," in *Proc. IEEE Int. Conf. Robot. Autom.*, 2016, pp. 909–916.

[3] C. D. Onal, M. T. Tolley, R. J. Wood, and D. Rus, "Origami-inspired printed robots," *IEEE/ASME Trans. Mechatronics*, vol. 20, no. 5, pp. 2214–2221, Oct. 2015.

[4] M. Salerno, K. Zhang, A. Menciassi, and J. S. Dai, "A novel 4-DOFs origami enabled, SMA actuated, robotic end-effector for minimally invasive surgery," in *Proc. IEEE Int. Conf. Robot. Autom.*, 2014, pp. 2844–2849.

[5] K. Miura, "Method of packaging and deployment of large membranes in space," *Inst. Space Astronaut. Sci. Rep.*, vol. 618, pp. 1–9, 1985.

[6] W. Fischer, G. Caprari, R. Siegwart, I. Thommen, W. Zesch, and R. Moser, "Foldable magnetic wheeled climbing robot for the inspection of gas turbines and similar environments with very narrow access holes," *Ind. Robot*, vol. 37, no. 3, pp. 244–249, 2010.

[7] G. Caprari *et al.*, "Highly compact robots for inspection of power plants," *J. Field Robot.*, vol. 29, no. 1, pp. 47–68, 2012.

[8] M. Savenkov and M. Turner, "New robotic technologies for inspecting two pole electric generators while the rotor remains in place," *J. Power Energy Eng.*, vol. 3, no. 4, pp. 123–127, 2015.

[9] T. Niino, T. Higuchi, and S. Egawa, "Dual excitation multiphase electrostatic drive," in *Proc. IEEE Ind. App. Conf.*, 1995, vol. 2, pp. 1318–1325.

[10] A. Yamamoto, T. Niino, and T. Higuchi, "Modeling and identification of an electrostatic motor," *Precis. Eng.*, vol. 30, no. 1, pp. 104–113, 2006.

[11] T. Hosobata, A. Yamamoto, and T. Higuchi, "Transparent synchronous electrostatic actuator for long-stroke planar motion," *IEEE/ASME Trans. Mechatronics*, vol. 20, no. 4, pp. 1765–1776, Aug. 2015.

[12] A. Yamamoto, T. Nakashima, and T. Higuchi, "Wall climbing mechanisms using electrostatic attraction generated by flexible electrodes," in *Proc. IEEE Int. Symp. Micro-Nano Mechatronics Human Sci.*, 2007, pp. 389–394.

[13] H. Prahlad, R. Pelrine, S. Stanford, J. Marlow, and R. Kornbluh, "Electroadhesive robots—wall climbing robots enabled by a novel, robust, and electrically controllable adhesion technology," in *Proc. IEEE Int. Conf. Robot. Autom.*, 2008, pp. 3028–3033.

[14] M. A. Graule *et al.*, "Perching and takeoff of a robotic insect on natural and artificial overhangs using switchable electrostatic adhesion," *Science*, vol. 352, no. 6288, pp. 978–982, 2016.

[15] C. D. Onal, R. J. Wood, and D. Rus, "Towards printable robotics: Origami-inspired planar fabrication of three-dimensional mechanisms," in *Proc. IEEE Int. Conf. Robot. Autom.*, 2011, pp. 4608–4613.

[16] A. O'Halloran, F. O'malley, and P. McHugh, "A review on dielectric elastomer actuators, technology, applications, and challenges," *J. Appl. Phys.*, vol. 104, no. 7, 2008, Art. no. 071101.

[17] M. Shahinpoor and K. J. Kim, "Ionic polymer-metal composites: I. Fundamentals," *Smart Mater. Struct.*, vol. 10, no. 4, pp. 819–833, 2001.

[18] S. Kim, M. Spenko, S. Trujillo, B. Heyneman, D. Santos, and M. R. Cutkosky, "Smooth vertical surface climbing with directional adhesion," *IEEE Trans. Robot.*, vol. 24, no. 1, pp. 65–74, Feb. 2008.

[19] H. Wang and A. Yamamoto, "A thin electroadhesive inchworm climbing robot driven by an electrostatic film actuator for inspection in a narrow gap," in *Proc. IEEE Symp. Safety, Security, Rescue Robot.*, 2013, pp. 1–6.

[20] H. Wang, A. Yamamoto, and T. Higuchi, "Electrostatic-motor-driven electroadhesive robot," in *Proc. IEEE/RSJ Int. Conf. Intell. Robots Syst.*, 2012, pp. 914–919.

[21] H. Wang, A. Yamamoto, and T. Higuchi, "A crawler climbing robot integrating electroadhesion and electrostatic actuation," *Int. J. Adv. Robot. Syst.*, vol. 11, pp. 1–11, 2014.

[22] S. P. Timoshenko and J. M. Gere, *Theory of Elastic Stability*. Tokyo, Japan: McGraw-Hill, 1961.

[23] X. Cheng, "Lateral instability of rectangular plates," *Appl. Math. Mech.*, vol. 10, no. 1, pp. 87–92, 1989.

[24] MO-B1001 from Misumi Electronics Corp., New Taipei City, Taiwan. 2016. [Online]. Available: http://www.misumi.com.tw/

[25] M. H. Rosen, G. le Pivain, R. Sahai, N. Jafferis, and R. J. Wood, "Development of a 3.2g untethered flapping-wing platform for flight energetics and control experiments," in *Proc. IEEE Int. Conf. Robot. Autom.*, 2016, pp. 3227–3233.

[26] A. Yamamoto, T. Nishijima, and T. Higuchi, "Deformable electrostatic linear motor," in *Proc. 1st IEEE Tech. Exhib. Based Conf. Robot. Autom.*, 2004, pp. 27–28.

Hongqiang Wang received the B.S. and M.S. degrees in mechanical engineering from Xi'an Jiaotong University, Xi'an, China, in 2008 and 2011, respectively, and the Ph.D. degree in precision engineering from University of Tokyo, Tokyo, Japan, in 2015.

Then, he was a Research Fellow in the Department of Biomedical Engineering and SINAPSE, National University of Singapore. Since October 2015, he has been a Postdoctoral Researcher in the School of Engineering and Applied Sciences and Wyss Institute, Harvard University, Cambridge, MA, USA. His research interests include soft robotics, surgical robotics, and novel actuators.

Akio Yamamoto received the B.S., M.S., and Ph.D. degrees in engineering from University of Tokyo, Tokyo, Japan in 1994, 1996 and 1999, respectively.

He has been an Associate Professor in the Department of Precision Engineering, University of Tokyo, since 2005. His research interests include actuators, haptics, and computer–human interactions.